Self-assembly of monodisperse graphene nanoribbons into submicron architectures with long-range order and uniform orientation

Jiangliang Yin[1], Daniel Pyle[1], Shinyoung Choi[1], Jeffrey R. Guest[2], Guangbin Dong[1]*
[1]Department of Chemistry, University of Chicago, Chicago, IL 60637, USA.
[2]Center for Nanoscale Materials, Argonne National Laboratory, Lemont, IL 60439, USA.

Abstract: Fabricating organic semi-conducting materials into large-scale well-organized architectures is critical for building high performance molecular electronics. While graphene nanoribbons (GNRs) hold enormous promise for various device applications, their assembly into a well-structured monolayer or multilayer architecture poses a substantial challenge. Here we report the preparation of length-defined monodisperse GNRs and their self-assembly into submicron-architectures with long-range order, uniform orientation as well as regular layers. The use of short alkyl side chains benefits forming stable multi-layers through interlocking structures. By changing the length and backbone shapes of these monodisperse GNRs, various three-dimensional assemblies including multilayer stripes, monolayer stripes, and nanowires, can be achieved, leading to different photophysical properties and band gaps. The discovery of these intriguing self-assembly behaviors of length-defined GNRs is expected to open the door for various future applications.

Introduction

The increasing demand in devising high-performance molecular electronics calls for semiconducting organic materials that exhibit well-defined large-scale structures with long-range order and uniform orientation[1-5]. Among various organic semiconductors, nanometer-wide strips of graphene, known as graphene nanoribbons (GNRs), have garnered enormous attention for their potential in various applications such as nanoelectronics, spintronics, photonics, sensing, quantum information processing, and energy conversion applications[6-12]. The synthesis of *structurally uniform GNRs* is an essential step for achieving well-defined self-assembled architectures. While top-down physical methods, realized by cutting graphene sheets[13], unzipping and squashing carbon nanotubes[14], are straightforward, these methods lack atomic precision, thus challenging to prepare GNRs with defined widths, lengths, edge structures, etc. The development of bottom-up synthesis techniques, using tailor-made polyarylene precursors prepared in solution or on metal surfaces, has enabled fabrication of atomically precise GNRs with well-controlled widths and edge structures[15-29], although the lengths and sequences of these ribbons are difficult to control[25, 27, 28]. More recently, Mateo-Alonso and co-workers realized an iterative condensation approach for preparing pyrene-pyrazoquinoxaline-based ribbons with precisely controlled lengths[30-34]. In addition, length-defined helical perylene diimide nanoribbons，acene derivatives, and thieno-fused coronene nanoribbons were reported by Nuckolls[35-39] and Mastalerz [40-43], respectively. The general strategy for fabrication of sequence- and length-controlled armchair GNRs, chevron GNRs, and their hybrids on surface was not realized until 2022 by us using a protecting-group-aided iterative synthesis (PAIS) approach[44], though this method is challenging to prepare monodisperse long GNRs. On the other hand, strategies such as edge functionalization[45-47] and nitrogen doping[48] have been developed to convert the superstructures of GNRs into nanowires, helices, nanofibers, three dimensional (3D) stacks, etc. However, arranging GNRs to architectures with precise long-range order and uniform orientation remains an unsolved problem (Fig. 1a).

In 2022, our group realized an integrated iterative binomial synthesis (IIBS) strategy to prepare long length-defined conjugated polymers from simple monomers containing two functional groups that can be activated by orthogonal methods (Fig. 1b)[49]. The exponential growth feature of the IIBS strategy offers an opportunity to synthesize long

and structurally uniform GNRs, whose large-scale self-assembly behaviors would be intriguing to study. Here we report our initial efforts in fabricating a series of monodisperse armchair GNRs (aGNRs) with either linear or kinked structures, which represents an efficient strategy to prepare long monodisperse GNRs, and further examining their self-assembly behaviors (Fig. 1c). Interestingly, these monodisperse GNRs show unique long-range order, uniform orientation, and selective layer formation.

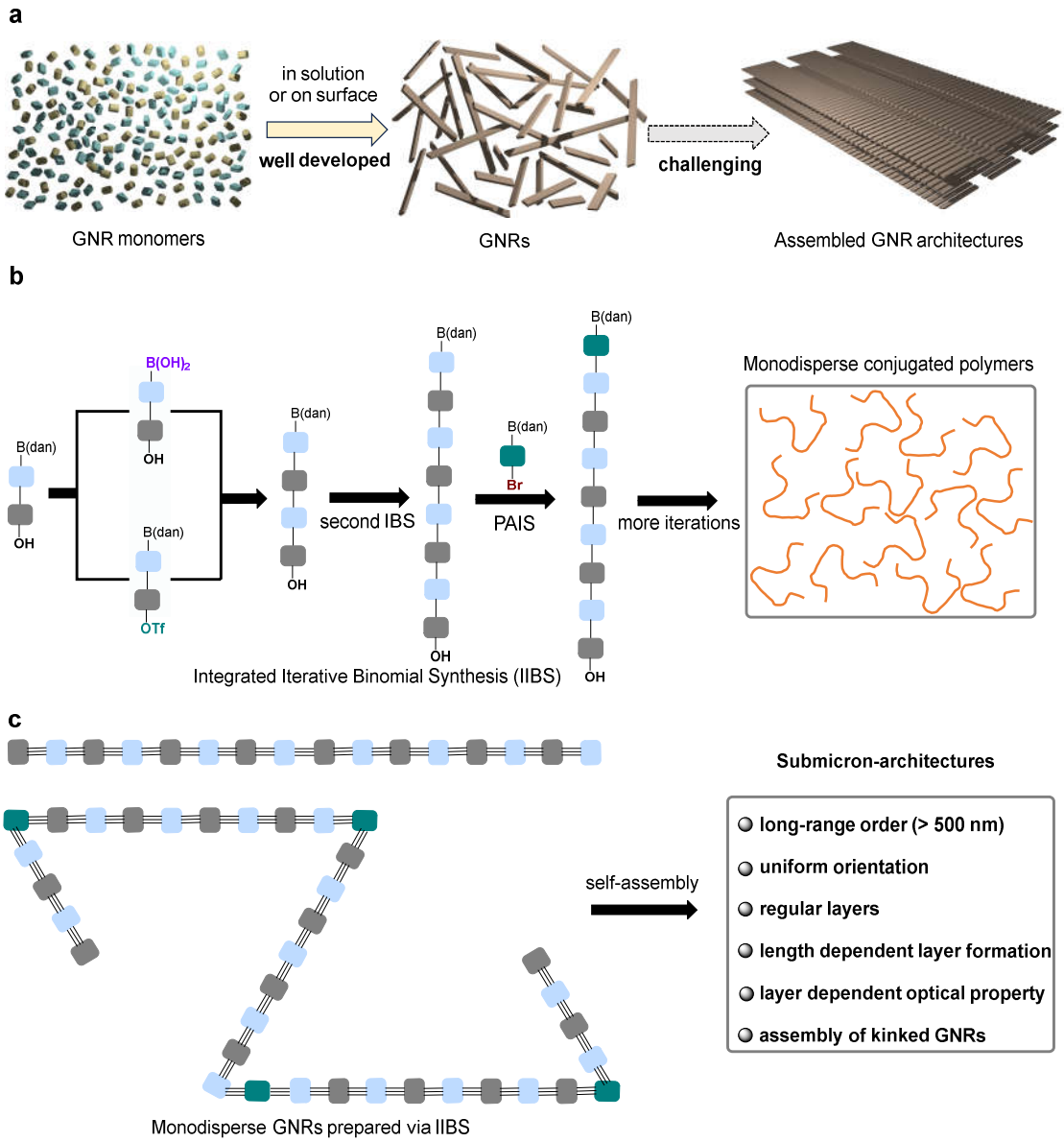

Fig. 1 | The journey to construct self-assembled GNR architectures with long-range order and uniform orientation. **a**, Current progress in constructing GNRs and challenges in constructing self-assembled GNR architectures with long-range order and uniform orientation. **b**, Development of integrated iterative binomial synthesis (IIBS) strategy to prepare monodisperse conjugated polymers. dan: 1,8-diaminonaphthalene. **c**, Fabrication of monodisperse linear or kinked GNRs and their self-assembly into submicron-architectures are developed in this work.

Results and discussion

Inspiration. In 2018, we developed the synthesis of a series of N = 6 aGNRs through solution A_2B_2 co-polymerization of *ortho*-terphenyl and *para*-phenylene-based monomers[50]. During this study, a model nanographene containing simple n-butyl groups as the side chains was prepared, and the x-ray crystallography showed that these side chains adopted an up-down oriented conformation (Fig. 2). Further analysis of the packing structure revealed that the effective length of the n-butyl groups (3.90 Å) in the armchair region surpassed the π-π stacking distance (3.48 Å), resulting in effective interlocking between two adjacent layers. Inspired by this observation, we conceived the question of whether stable three-dimensional GNR architectures could be realized by choosing suitable side chains and unifying the lengths.

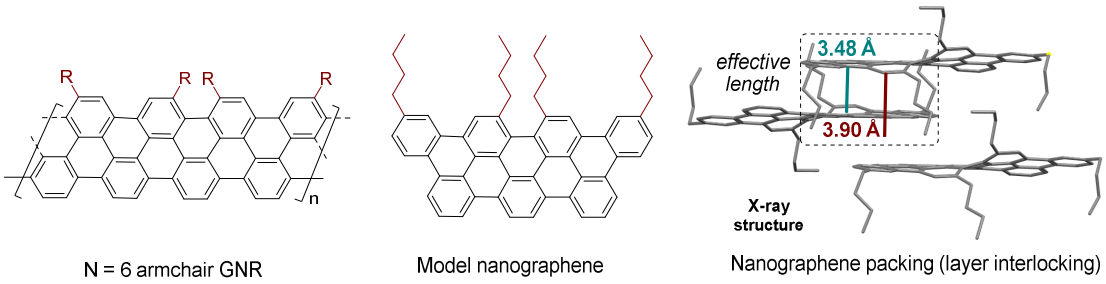

Fig. 2 | Inspiration from the packing structure of a well-defined nanographene.

Self-assembly of polydisperse GNRs. To explore this idea, the synthesis of polydisperse N = 6 aGNR polymer precursor with n-butyl side chains was first pursued (Fig. 3a). Under the $Pd(P^tBu_3)_2/K_3PO_4$ catalysis conditions, Suzuki polymerization of n-butyl-substituted *ortho*-terphenyl dibromide (**M1**) with bispinacol borate (**M2**) provided the desired GNR polymer precursor **P1** in 86% yield after Soxhlet extraction with boiling acetone (Supplementary Fig. S1). Due to its good solubility in normal organic solvents (such as CH_2Cl_2), the obtained polymer was successfully characterized by $^1H/^{13}C$ nuclear magnetic resonance (NMR) spectroscopy, gel permeation chromatography (GPC), matrix-assisted laser desorption/ionization-time of flight mass spectrometry (MALDI-TOF-MS), and Fourier-transform infrared spectroscopy (FT-IR), showing high molecular weight and relatively low polydispersity index (PDI)(1.73) (Fig. 3b and 3c, Supplementary Table S1). Subsequently, slow addition of TfOH (triflic acid) into a solution of **P1** and 2,3-dichloro-5,6-dicyano-1,4-benzoquinone (DDQ) in dry CH_2Cl_2 at 0 °C led to the formation of the desired GNR **G1** as a black solid in high yield. The resulting **G1** can be well dispersed in toluene, THF (tetrahydrofuran) and NMP (*N*-methylpyrrolidone), rendering the successful characterization by FT-IR,

Raman, UV-Vis-NIR spectroscopy and atomic force microscopy (AFM). FT-IR analysis suggested the effective cyclodehydrogenation of the polyphenylene backbones to GNR core structures, displaying a clear disappearance/attenuation of several peaks (3083, 3048, 3023, 2997 cm^{-1}) from the aryl C–H stretching vibrations and the out-of-plane (opla) C–H deformation bands (818 cm^{-1}) for typical mono- and disubstituted benzene rings[51]. Raman spectroscopy of **G1** showed two intense peaks around 1337 and 1595 cm^{-1}, assigned to D and G bands of graphitic materials, respectively (Fig. 3d). Three second-order bands (2D, D + G and 2 G) were also detected for **G1**. The bimodal D band and the significantly broadened 2D band suggested stronger aggregation via a π–π stacking interaction[52]. AFM measurements were performed to gain the detailed information on the self-assembly behavior of **G1**. Fig. 3e shows an AFM image of monolayer GNR deposited on highly oriented pyrolytic graphite (HOPG). Different from the previously reported N = 6 aGNR with longer and more branching side chains[50], which gave monolayer striped domains, **G1** self-assembled into large-scale monolayer 2D stripes in the sparse area. The length of these strips was found to be 200-300 nm, while their width varied probably due to the polymeric character of this sample. In the dense area, these GNRs formed multilayer stripes with lengths of 200-300 nm and heights of 5-15 nm, which could benefit from the layer interlocking by the n-butyl side chains (Fig. 3f). To explore how such aggregation affects the photophysical properties, UV–Vis–NIR measurements were next conducted in solutions of *N*-methylpyrrolidone (NMP) at room temperature. As illustrated in Fig. 3g, the polymeric GNR displays broad absorption across the UV, visible, and near-IR (NIR) regions with blunt absorption onsets. Employing the Tauc Method, the optical band gap of a low concentration sample in the NMP solution was determined to be 1.18 eV, akin to the reported N = 6 aGNRs with other types of side chains[50]. As anticipated, a normal concentration of the same sample led to a drop in the optical band gap to 0.95 eV, likely owing to the multilayer aggregation[53,54].

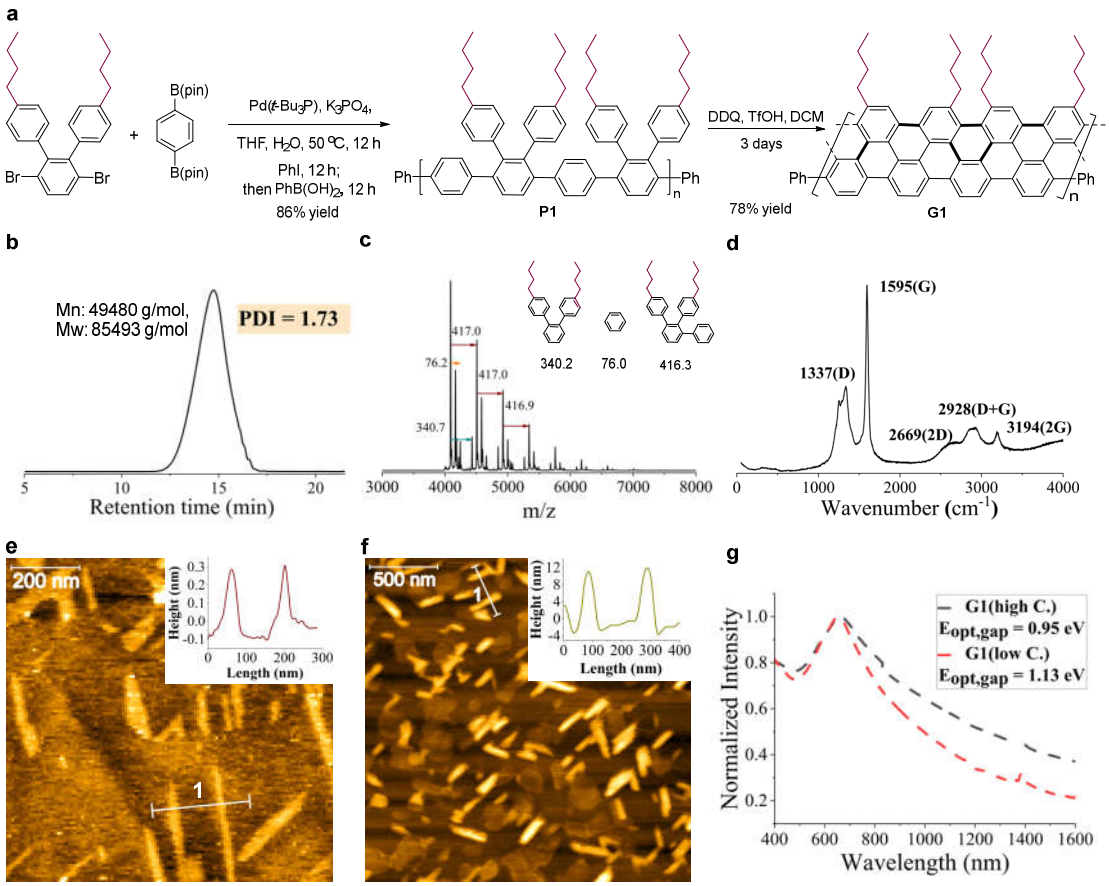

Fig. 3 | Investigation of the self-assembly of polydisperse N = 6 aGNR with n-butyl side chains. **a**, Synthetic pathway for **G1** using Suzuki polymerization. **b**, GPC trace of the GNR precursor **P1**. **c**, MALDI-TOF-MS spectrum of **P1**. **d**, Raman spectrum of **G1**. **e**, AFM image of **G1** on HOPG showing monolayer aggregation. Inset: cross-sectional profiles of line 1. **f**, AFM image of **G1** on HOPG showing multilayer aggregation. Inset: cross-sectional profiles of line 1. **g**, UV–vis spectra of **G1** in NMP solution at high concentration (0.1 mg in 5 mL NMP, black) and at low concentration (the same solution after precipitation under N_2 for 24 h, red).

Self-assembly of length-defined linear GNRs. To enhance the shape regularity of the assembly, synthesis of length-defined N = 6 aGNR was next conducted. Using the IIBS approach, the length-defined N = 6 aGNR polymer precursors can be obtained after a defined number of rounds of iteration, followed by a sequence of 1,8-diaminonaphthalene (dan)-masked boronic acid (B(dan)) deprotection, oxidation, triflation and end capping (Fig. 4a and 4b, and Supplementary Information). The single and sharp peak from the GPC trace of polymer **P2** with 34 phenylene units in its backbone indicates a small PDI (1.03) (Fig. 4c), which together with the MALDI data supports the expected length-defined character (Supplementary Fig. S6). The monodisperse **P2** was subsequently "graphitized" into **G2**, through the oxidative cyclodehydrogenation using DDQ/TfOH in dichloromethane. **G2** was initially

characterized by FT-IR and Raman spectroscopy, revealing the successful cyclodehydrogenation (Supplementary Information). In order to investigate the self-assembly behavior of length-defined **G2**, its dispersion in toluene was drop-cast over freshly peeled graphite surface. AFM imaging revealed that **G2** can form long-range organized multilayer stripes with lengths of 300-600 nm (Fig. 4e). Firstly, line profiles (line 1 and line 2) across the stripes in the overview AFM image show that the heights of these stripes are around 1-3 nm, revealing the formation of multilayers (Fig. 4f and 4g). Secondly, the average periodicity of these stripes is 8.1 nm, as shown by a line profile across the line 2 (Fig. 4g). The interstripe distance is close to the length of **G2** and more than eight times of its width. Such assembly behavior is different from all previously reported GNR assemblies[15-16,21-23,45-48,50-51]. Considering the sizes of highly ordered stripes and the GNRs as well as the synergistic effect of the π–π interaction, an aggregation model for **G2** is proposed in Fig. 4h and 4i. The up-down oriented n-butyl side chains can efficiently promote the vertical stacking of the adjacent GNR backbones, resulting in the formation of multilayer architectures, in an entropically driven side-by-side and end-to-end fashion. In the sparse area, monolayer stripes were also observed, showing rectangle shapes with clean edges (see Supplementary Information). The formation of these stripes with unprecedented long-range order, uniform orientation as well as regular layers, suggests the unique assembly feature of monodisperse GNRs. UV–Vis–NIR spectra of **G2** under different concentrations reveal the effect of this multilayer aggregation in substantially decreasing the optical band gap from 1.07 eV to 0.76 eV (Fig. 4d).

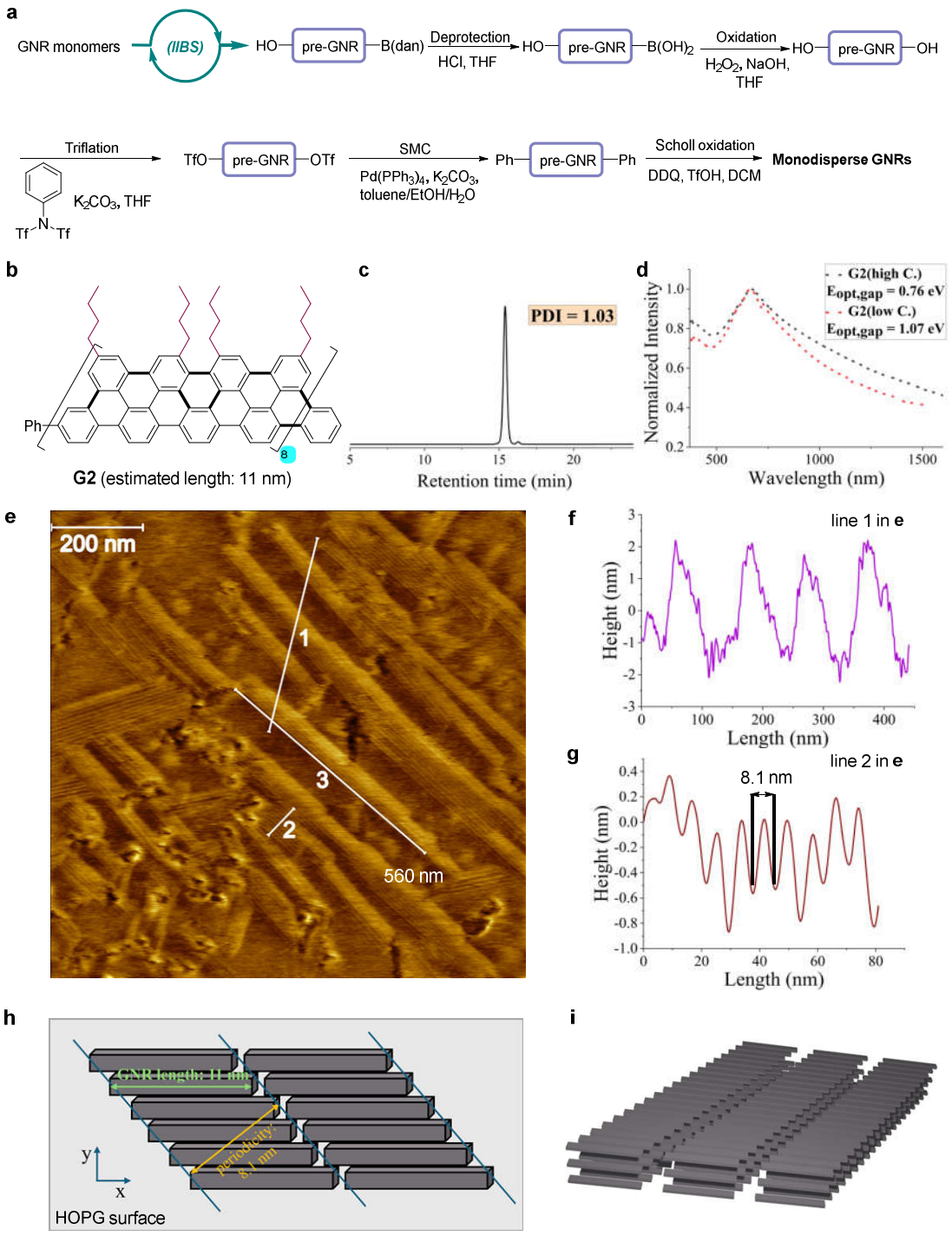

Fig. 4 | Investigation of the self-assembly of length-defined N = 6 aGNR with n-butyl side chains. a, General synthetic route towards monodisperse GNRs. SMC, Suzuki–Miyaura coupling. **b**, Chemical structure of length-defined GNR **G2** with 34 phenylene units on its backbone. **c**, GPC trace of the GNR precursor **P2** showing its monodispersity. **d**, UV–vis spectra of **G2** in NMP solution at high concentration (0.1 mg in 5 mL NMP, black) and at low concentration (the same solution after precipitation under N_2 for 24 h, red). **e**, AFM image of **G2** on HOPG showing the formation of organized multilayer assemblies. **f**, **g** Cross-sectional profiles of the image (along line 1 and line 2 in **e**), respectively. **h**, Proposed monolayer aggregation model of **G2**. **i**, Proposed multilayer aggregation model of **G2**.

To evaluate the length effect to the self-assembly behaviors of monodisperse GNRs, a nearly double lengthened N = 6 aGNR, **G3** with 66 phenylene units on its backbone was prepared by similar procedures (Fig. 5a and Supplementary Information). From the GPC trace of precursor **P3**, the PDI was determined as 1.03, which is consistent with the unimolecular nature of this polymer (Fig. 5b). FT-IR and Raman measurements of **G3** confirmed the expected cyclodehydrogenation (see Supplementary Information). Although **G3** is much longer than **G2**, **G3** is still soluble in toluene and NMP after mild sonication, generating stable dark green dispersions without observable precipitate, which facilitated the AFM and UV-Vis-NIR measurements. Interestingly, unlike **G2**, the deposition of **G3** in the same way reproducibly provided self-assembled monolayer strips of rectangle shapes and clean edges (Fig. 5d). The lengths of these rectangles vary, ranging from fifty nanometers to a few hundred nanometers. Notably, according to the representative domains, the observed widths of these rectangles are 41.9 nm, 63.2 nm, 81.1 nm, and 101.0 nm, indicating a discrete rather than continuous distribution (Fig. 5e, 5f, 5g, and 5h). The average difference among these widths is approximately 20 nm, which correlates well with the estimated length of the individual aGNRs; this is also consistent with the findings of **G2**. The intriguing monolayer assembly of **G3** might be attributed to its notably extended length, adding difficulties for interlayer locking. The absence of multilayer assembly with longer monodisperse GNRs indicates that altering the ribbon length can greatly affect their supramolecular architecture. The optical band gap of aggregated **G3** is approximately 0.94 eV (Fig. 5c), substantially higher than that of **G2** (0.76 eV), indicating the influence of multilayer aggregation on their optical behaviors.

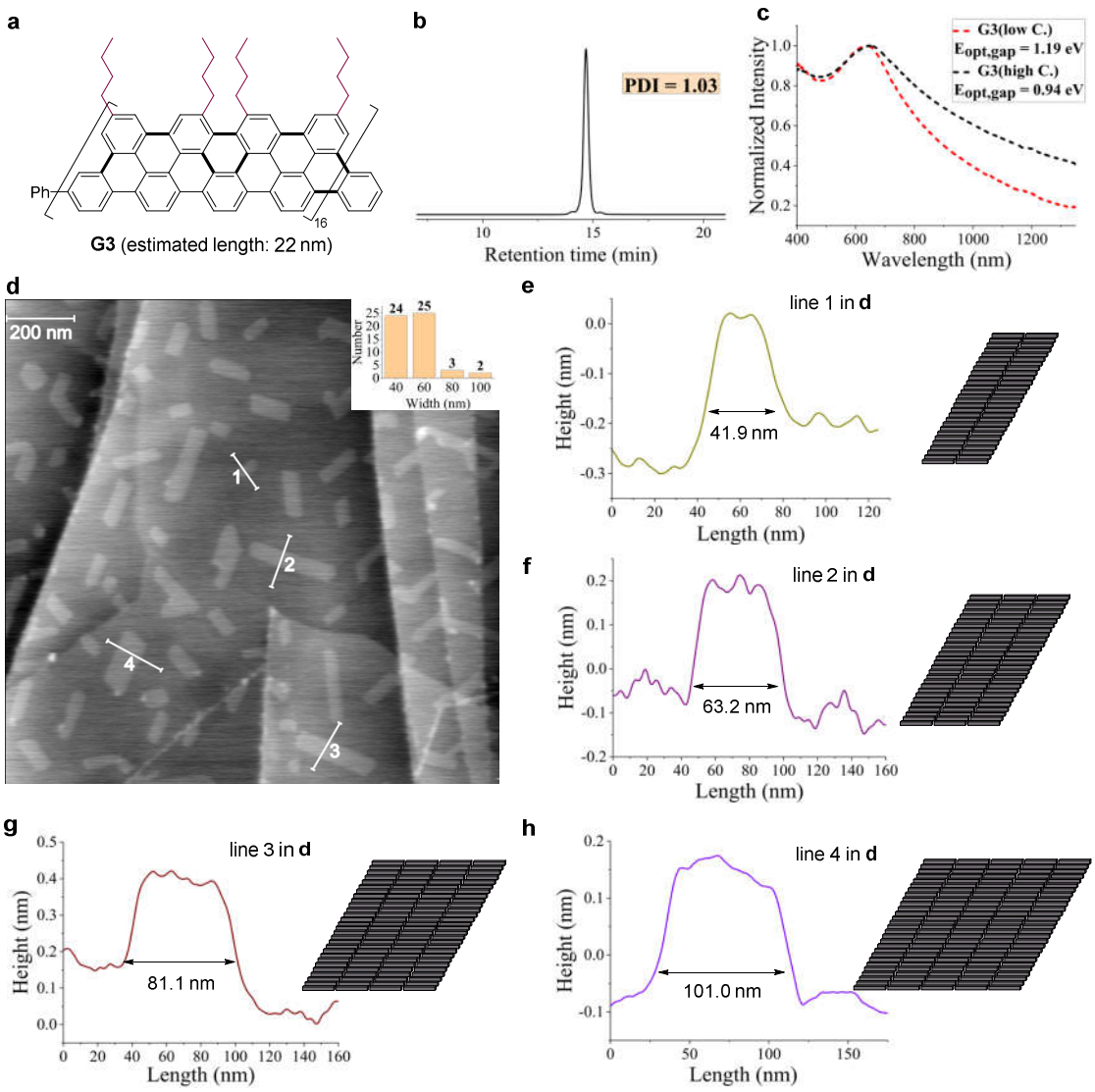

Fig. 5 | Investigation of the self-assembly of longer monodisperse N = 6 aGNR with n-butyl side chains. a, Chemical structure of longer N = 6 aGNR **G3** with 66 phenylene units on its backbone. **b**, GPC trace of the GNR precursor **P3** showing its unimolecular nature. **c**, UV–vis spectra of **G3** in NMP solution at high concentration (0.1 mg in 5 mL NMP, black) and at low concentration (the same solution after precipitation under N_2 for 24 h, red). **d**, AFM image of **G3** on HOPG showing the formation of organized monolayer assemblies. Inset: Statistical analysis of the widths of assemblies. **e**, **f**, **g**, **h**, Cross-sectional profiles of the image (along line 1, 2, 3, and 4 in **d**).

Self-assembly of kinked monodisperse GNRs. Having recognized that monodisperse GNRs with different lengths can form different large-scale submicron architectures, we next explore the influence of backbone shapes on their assembly behaviors. To the end, monodisperse GNR precursor **P4** was synthesized via a similar IIBS/end-capping protocol (Fig. 6 and Supplementary Information), in which four 120° kinks were introduced to the N = 6 aGNR backbone to give a Z-shape polymer. GPC trace of **P4** indicates an extremely narrow PDI (1.02), suggesting the unimolecular nature (Fig. 6b).

The efficiency of the cyclodehydrogenation process was confirmed by FT-IR and Raman measurements (see Supplementary Information). Despite that **P4** contains 136 phenylene units in its backbone, the resulting **G4** exhibits solubility comparable to that of other GNRs, likely owing to its kinked structure. Although kinked structures are generally not favorable for self-assembly, **G4** unexpectedly formed well organized nanowires with lengths of 200-800 nm based on the AFM images (Fig. 6d and Supplementary Fig. S29). The intersection angles between these nanowires are either 60° or 120°, aligning well with the introduced kinks. Monolayer stripes were also observed with average periodicity of 11.0 nm, probably representing the effective length of **G4** (Fig. 6e). The width of these nanowires is twice the effective length of **G4**, suggesting that two GNRs were likely assembled in parallel (Fig. 6f). Additionally, a line profile along these nanowires reveals a periodicity of 6.2 nm, matching closely with the calculated effective width of **G4** (Fig. 6g). Based on these experimental results, an assembly model was proposed for **G4** as shown in Fig. 6h. The longer edges of **G4** prefer to stick together to form monolayer or multilayer stripes with observed periodicity, whereas the 60° or 120° angles could be possibly generated when the long edge of a GNR aggregates with the short edge of another GNR during their assembling. Meanwhile, some disordered areas were also observed, possibly due to the formation of alternative assemblies or isomers resulting from the rotational kinks during the Scholl oxidation process. The UV–Vis–NIR spectra revealed an optical band gap of 0.99 eV (Fig. 6c), indicating weak aggregation of kinked GNRs in solution.

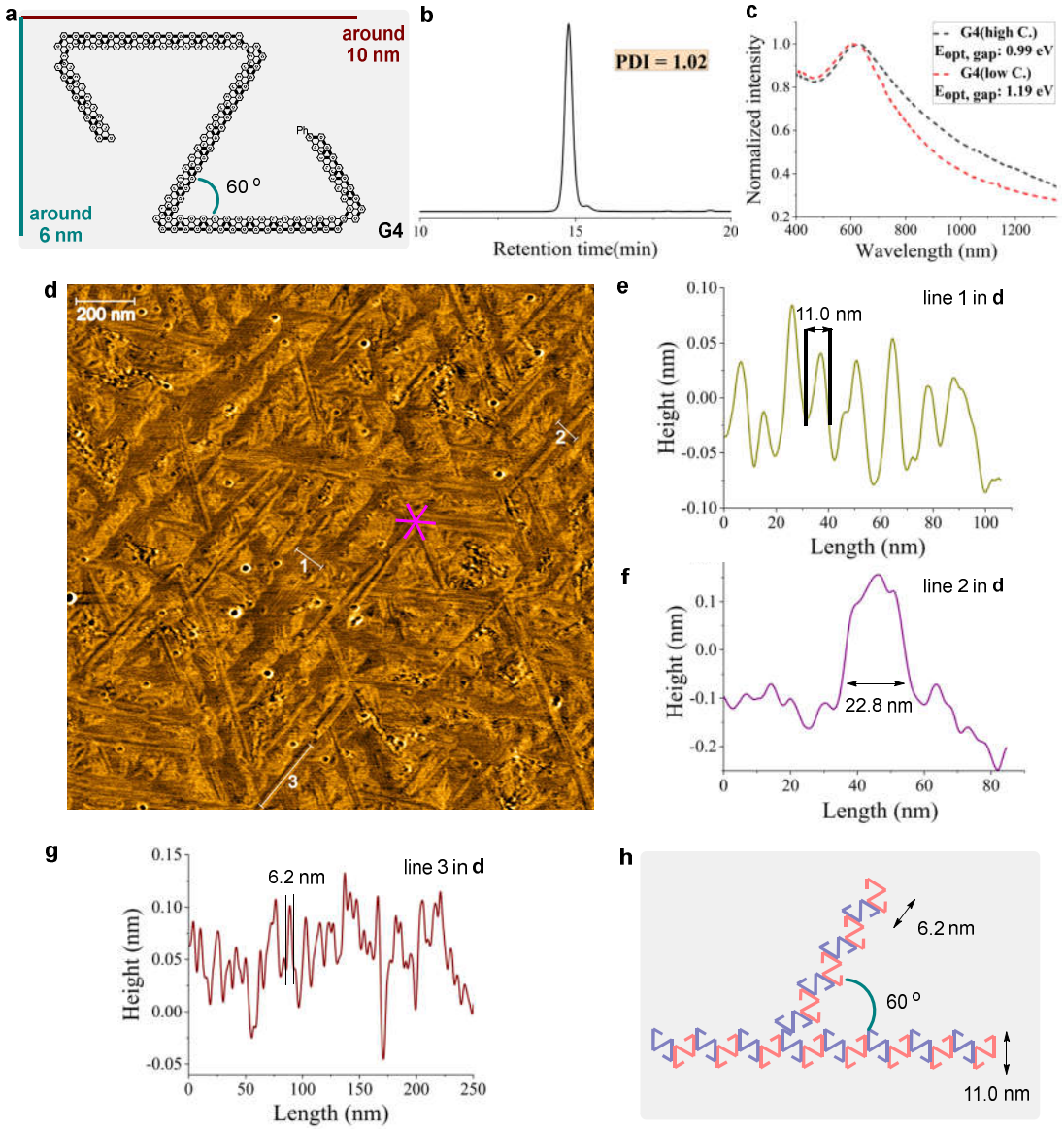

Fig. 6 | Investigation of the self-assembly of kinked monodisperse N = 6 aGNR with n-butyl side chains. **a**, Chemical structure of kinked N = 6 aGNR **G4** (Side chains are omitted for better clarity). **b**, GPC trace of the kinked GNR precursor **P4** showing its unimolecular nature. **c**, UV–vis spectra of **G4** in NMP solution at high concentration (0.1 mg in 5 mL NMP, black) and at low concentration (the same solution after precipitation under N_2 for 24 h, red). **d**, AFM image of **G4** on HOPG showing the formation of organized monolayer or double layer nanowires. **e**, **f**, **g**, Cross-sectional profiles of the image (along line 1, 2, and 3 in **d**). **h**, Proposed aggregation model of **G4**.

Conclusions

In summary, we have developed a general approach to prepare long length-defined monodisperse aGNRs (up to >20 nm) and discovered that they can assemble into submicron-architectures with long-range order, uniform orientation as well as regular layers. The use of n-butyl side chains promotes forming interlocking structures, leading to stable three-dimensional GNR assembly. Formation of these superstructures, such as

multilayer stripes, monolayer stripes, and nanowires, is tunable by varying the GNR length and topology, which makes convenient to engineer the photophysical properties and band gaps of these materials. Ongoing efforts include exploring device applications of these aggregated ribbons and using this strategy to study more diverse architectures based on other GNRs.

Methods

Synthesis. Experimental details and characterization data (^{1}H NMR, ^{13}C NMR, MALDI-TOF-MS etc.) for all products can be found in Supplementary Information.

Characterization and imaging of graphene nanoribbons. Experimental details for spectroscopic analyses and microscopic tools can be found in Supplementary Information.

Data availability

The data that support the findings of this study are available within the article and its Supplementary Information. Source data are provided with this paper.

References

1. Whitesides, G. M., Mathias, J. P., & Seto, C.T. Molecular self-assembly and nanochemistry: a chemical strategy for the synthesis of nanostructures. *Science* **254**, 1312-1319 (1991).
2. Whitesides, G. M. & Boncheva, M. Beyond molecules: self-assembly of mesoscopic and macroscopic components. *Proc. Natl. Acad. Sci. U.S.A.* **99**, 4769–4774 (2002).
3. Lombardo, D., Calandra, P., Pasqua, L. & Magazù, S. Self-assembly of organic nanomaterials and biomaterials: the bottom-up approach for functional nanostructures formation and advanced applications. *Materials* **13**, 1048 (2020).
4. Yao, Z.-F., Wang, J.-Y. & Pei, J. High-performance polymer field-effect transistors: from the perspective of multi-level microstructures. *Chem. Sci.* **12**, 1193 (2021).
5. Yuan, M. et al. Molecular Electronics: From nanostructure assembly to device integration. *J. Am. Chem. Soc.* **146**, 7885–7904 (2024).
6. Son, Y.-W., Cohen M. L. & Louie, S. G. Half-metallic graphene nanoribbons. *Nature* **444**, 347 (2006).
7. Wu, J., Pisula, W. & Müllen, K. Graphenes as potential material for electronics. *Chem. Rev.* **107**, 718 (2007).
8. Li, X., Wang, X., Zhang, L., Lee, S. & Dai, H. Chemically derived, ultrasmooth graphene nanoribbon semiconductors. *Science* **319**, 1229 (2008).
9. Prezzi, D., Varsano, D., Ruini, A., Marini, A. & Molinari, E. Optical properties of graphene nanoribbons: The role of many-body effects. *Phys. Rev. B* **77**, 041404(R) (2008).

10. Ritter, K. A. & Lyding, J. W. The influence of edge structure on the electronic properties of graphene quantum dots and nanoribbons. *Nat. Mater.* **8**, 235 (2009).
11. Ruffieux, P. *et al*. On-surface synthesis of graphene nanoribbons with zigzag edge topology. *Nature* **531**, 489 (2016).
12. Blackwell, R. E. *et al*. Spin splitting of dopant edge state in magnetic zigzag graphene nanoribbons. *Nature* **600**, 647 (2021).
13. Chen, Z., Lin, Y.-M., Rooks, M. J. & Avouris, P. Graphene nano-ribbon electronics. *Phys. E* **40**, 228–232 (2007).
14. Kosynkin, D. V. et al. Longitudinal unzipping of carbon nanotubes to form graphene nanoribbons. *Nature* **458**, 872–876 (2009).
15. Narita, A., Wang, X.-Y., Feng, X. & Müllen, K. New advances in nanographene chemistry. *Chem. Soc. Rev.* **44**, 6616 (2015).
16. Narita, A., Feng, X. & Müllen, K. Bottom-up Synthesis of Chemically Precise Graphene Nanoribbons. *Chem. Rec.* **15**, 295 (2015).
17. Talirz, L., Ruffieux, P. & Fasel, R. On-surface synthesis of atomically precise graphene nanoribbons. *Adv. Mater.* **28**, 6222 (2016).
18. Houtsma, R. S. K., de la Rie, J. & Stöhr, M. Atomically precise graphene nanoribbons: interplay of structural and electronic properties. *Chem. Soc. Rev.* **50**, 6541 (2021).
19. Liu, Z. et al. Small size, big impact: recent progress in bottom-up synthesized nanographenes for optoelectronic and energy applications. *Adv. Sci.* **9**, 2106055 (2022).
20. Zhou X. & Yu G. Modified engineering of graphene nanoribbons prepared via on-surface synthesis. *Adv. Mater.* **32**, 1905957 (2020).
21. Yano, Y., Mitoma, N., Ito, H. & Itami, K. A quest for structurally uniform graphene nanoribbons: Synthesis, properties, and applications. *J. Org. Chem.* **85**, 4. (2020).
22. Yoon, K.-Y. & Dong G. Liquid-phase bottom-up synthesis of graphene nanoribbons. *Mater. Chem. Front.* **4**, 29 (2020).
23. Jolly, A., Miao, D., Daigle, M. & Morin, J.-F. Emerging bottom-up strategies for the synthesis of graphene nanoribbons and related structures. *Angew. Chem. Int. Ed.* **59**, 4624 (2020).
24. Gu, Y., Qiu, Z. & Müllen, K. Nanographenes and graphene nanoribbons as multitalents of present and future materials science. *J. Am. Chem. Soc.* **144**, 11499–11524 (2022).
25. Von Kugelgen, S. et al. Templated synthesis of end-functionalized graphene nanoribbons through living ring-opening alkyne metathesis polymerization. *J. Am. Chem. Soc.* **141**, 11050–11058 (2019).
26. Yao, X. et al. Synthesis of nonplanar graphene nanoribbon with fjord edges. *J. Am. Chem. Soc.* **143**, 5654–5658 (2021).
27. Lee, J., Ryu, H., Park, S., Cho, M. & Choi, T.-L. Living Suzuki–Miyaura catalyst-transfer polymerization for precision synthesis of length-controlled armchair graphene nanoribbons and their block copolymers. *J. Am. Chem. Soc.* **145**, 15488–15495 (2023).
28. Pun, S. H., Delgado, A., Dadich, C., Cronin, A. & Fischer, F. R. Controlled catalyst-transfer polymerization in graphene nanoribbon synthesis. *Chem* **10**, 675–685 (2024).

29. Liu, K. et al. Cove-edged chiral graphene nanoribbons with chirality-dependent bandgap and carrier mobility. *J. Am. Chem. Soc.* **146**, 1026–1034 (2024).
30. Cortizo-Lacalle, D. et al. Monodisperse N-doped graphene nanoribbons reaching 7.7 nanometers in length. *Angew. Chem. Int. Ed.* **57**, 703 (2018).
31. Dubey, R. K., Melle-Franco, M. & Mateo-Alonso, A. Twisted molecular nanoribbons with up to 53 linearly-fused rings. *J. Am. Chem. Soc.* **143**, 6593–6600 (2021).
32. Hernández-Culebras, F., Melle-Franco, M. & Mateo-Alonso, A. Doubling the length of the longest pyrene-pyrazinoquinoxaline molecular nanoribbons. *Angew. Chem. Int. Ed.* **61**, e202205018 (2022).
33. Dubey, R. K. et al. Accelerated iterative synthesis of ultralong graphene nanoribbons with full atomic precision. *Chem* **9**, 2983–2996 (2023).
34. Marongiu, M. et al. Molecular graphene nanoribbon junctions. *J. Am. Chem. Soc.* **146**, 3963–3973 (2024).
35. Zhong, Y. et al. Helical ribbons for molecular electronics. *J. Am. Chem. Soc.* **136**, 8122 (2014).
36. Sisto, T. J. et al. Long, atomically precise donor–acceptor cove-edge nanoribbons as electron acceptors. *J. Am. Chem. Soc.* **139**, 5648 (2017).
37. Schuster, N. J. et al. A helicene nanoribbon with greatly amplified chirality. *J. Am. Chem. Soc.* **140**, 6235 (2018).
38. Xiao X. *et al*. Chirality amplified: long, discrete helicene nanoribbons. *J. Am. Chem. Soc.* **143**, 983 (2021).
39. Jin, Z. et al. Iterative synthesis of contorted macromolecular ladders for fast-charging and long-life lithium batteries. *J. Am. Chem. Soc.* **144**, 13973–13980 (2022).
40. Kohl, B., Rominger, F. & Mastalerz, M. A pyrene-fused N-heteroacene with eleven rectilinearly Annulated aromatic rings. *Angew. Chem. Int. Ed.* **54**, 6051 (2015).
41. Yang, X., Rominger, F. & Mastalerz, M. Benzo-fused perylene oligomers with up to 13 linearly annulated rings. *Angew. Chem. Int. Ed.* **60**, 7941 (2021).
42. Yang, X., Brückner, M., Rominger, F., Kirschbaum, T. & Mastalerz, M. Dispersion-driven formation of chiral twisted PAH double helices. *Chem* **10**, 832 (2024).
43. Yang, X., Elbert, S. M., Rominger, F. & Mastalerz, M. A series of soluble thieno-fused coronene nanoribbons of precise lengths. *J. Am. Chem. Soc.* **144**, 9883–9892 (2022).
44. Yin, J., Jacobse, P. H., Pyle, D., Wang, Z., Crommie, M. F. & Dong, G. Programmable fabrication of monodisperse graphene nanoribbons via deterministic iterative synthesis. *J. Am. Chem. Soc.* **144**, 16012–16019 (2022).
45. Keerthi, A. et al. Edge functionalization of structurally defined graphene nanoribbons for modulating the self-assembled structures. *J. Am. Chem. Soc.* **139**, 16454–16457 (2017).

46. Xu, F. et al. Tunable superstructures of dendronized graphene nanoribbons in liquid phase. *J. Am. Chem. Soc.* **141**, 10972–10977 (2019).
47. Ohtomo, M. et al. Interpolymer self-assembly of bottom-up graphene nanoribbons fabricated from fluorinated precursors. *ACS Appl. Mater. Interfaces* **10**, 31623–31630 (2018).
48. Vo, T. H. et al. Nitrogen-doping induced self-assembly of graphene nanoribbon-based two-dimensional and three-dimensional metamaterials. *Nano Lett.* **15**, 5770–5777 (2015).
49. Yin, J., Choi, S., Pyle, D., Guest, J. R. & Dong, G. Backbone engineering of monodisperse conjugated polymers via integrated iterative binomial synthesis. *J. Am. Chem. Soc.* **145**, 19120–19128 (2023).
50. Li, G. *et al*. A modular synthetic approach for band-gap engineering of armchair graphene nanoribbons. *Nat. Commun.* **9**, 1687 (2018).
51. Narita, A. et al. Synthesis of structurally well-defined and liquid-phase-processable graphene nanoribbons. *Nat. Chem.* **6**, 126–132 (2014).
52. Malard, L. M., Pimenta, M. A., Dresselhaus, G. & Dresselhaus, M. S. Raman spectroscopy in graphene. *Phys. Rep.* **473**, 51–87 (2009).
53. Vo, T. H. et al. Large-scale solution synthesis of narrow graphene nanoribbons. *Nat. Commun.* **5**, 3189 (2014).
54. Negishi, R. et al. Crossover point of the field effect transistor and interconnect applications in turbostratic multilayer graphene nanoribbon channel. *Sci. Rep.* **11**, 10206 (2021).

Acknowledgements

This research was supported by the Office of Naval Research MURI Program N00014-19-1-2596. Work performed at the Center for Nanoscale Materials, Argonne National Laboratory, a U.S. Department of Energy Office of Science User Facility, was supported by the U.S. DOE, Office of Basic Energy Sciences, under Contract No. DE-AC02-06CH11357.

Author contributions

J. Y. designed, synthesized, and characterized the GNRs. J. Y. and D. P. conducted the AFM measurements. S. C. conducted the Raman measurements. J. Y., D. P., and S. C. performed data analysis. J. R. G. supervised the AFM measurements and helped to interpret the results. All authors contributed to the scientific discussion and writing the manuscript. G. D. directed the project.

Additional information

Supplementary information is available in the online version of the paper. Reprints and permissions information is available online at www.nature.com/reprints. Publisher's note: Springer Nature remains neutral with regard to jurisdictional claims in published maps and institutional affiliations. Correspondence and requests for materials should be addressed to G. D.

Competing interests

The authors declare no competing interests.